Electronic structure of silicon nanowires: A photoemission and x-ray absorption study

Y. F. Zhang, L. S. Liao, W. H. Chan, and S. T. Lee
Department of Physics and Materials Science, City University of Hong Kong, Hong Kong, China

R. Sammynaiken
Department of Chemistry, University of Western Ontario, London, Ontario, Canada N6A 5B7

T. K. Sham
Department of Physics and Materials Science, City University of Hong Kong, Hong Kong, China and Department of Chemistry, University of Western Ontario, London, Ontario, Canada N6A 5B7

(Received 24 June 1999; revised manuscript received 31 August 1999)

Photoemission and x-ray absorption spectroscopy have been used to study silicon nanowires prepared by a laser ablation technique together with Si(100) and porous silicon. Si 2p and valence-band spectra show that the Si nanowires are essentially crystalline Si encapsulated by silicon oxide. HF etching removes the surface oxide but leaves the morphology intact. Si K-edge x-ray absorption near-edge structures show that the characteristic Si K-edge whiteline doublet in Si(100) smears out in the nanowires and blurs entirely in porous silicon and that the whiteline exhibits a small blueshift. This observation indicate a progressive degradation in long-range order going from bulk Si to nanowires to porous Si and a wider band gap for a fraction of the nanowires. The extended x-ray absorption fine structures show that despite an increased disorder relative to bulk Si, Si nanowire remains essentially crystalline, in good accord with recent transmission electron microscopy and x-ray powder diffraction studies.

I. INTRODUCTION

The electronic structure of silicon in unusually dimensions (surface, interface, quantum wires, quantum dots, etc.) is of considerable interest both fundamentally and technologically. The study of nanostructure silicon in particular has been an area of intense interest in recent years.[1–11] This is partly because nanosize materials are likely to exhibit electronic structure different from the bulk due to a combined effect of surface, interface, and quantum confinement, and partly because of the increasing demand in application of nanoscaled silicon in many advanced technologies.

The advancement in nanostructure studies is due largely to the advancement in the preparation methodology of the materials as well as the use of advanced characterization and computational techniques. Compared to the study of carbon nanotubes, the study of Si nanowires has been hampered by the lack of bulk quantity of nanowire and hence has been limited to the study of porous silicon (PS).[6,7] PS is a spongelike interconnecting Si wire network with pillars and nodules of nanometer dimensions. Its study drew enormous attention since it was found that PS emits intense visible luminescence at room temperature.[6]

A recently reported preparation of silicon nanowires[1,2,4] has greatly changed the scope of Si nanowire research. The preparation of bulk quantities of silicon wires using a laser ablation technique at high temperature makes it possible to study these materials in some details.[1,3,4,6,7] It has been shown that this method produces a distribution of fiberlike free-standing wires having diameters varying from 3 to ~40 nm with lengths up to a few hundred microns and that silicon oxides play a crucial role in the synthesis. Transmission electron microscopy (TEM) and x-ray powder diffraction (XRD) show that these wires are essentially crystalline Si with many defects and they are always encapsulated with a thin layer of silicon oxides.[1,3,4] Nanoparticles of Si chains linked by amorphous Si oxide are sometimes found coexisting with Si wires.[4] The Si nanowires thus prepared generally exhibit photoluminescence somewhat similar to those of porous silicon.[5]

Despite considerable morphology and structural studies, information on the electronic structure of these materials is relatively lacking. In this paper we report on a photoemission spectroscopy (PES) and x-ray absorption fine-structures (XAFS) study of Si nanowires prepared by the laser ablation method as well as a p type Si(100) wafer and a porous silicon sample prepared from a p-type Si(100) wafer (~10 Ω cm). PES probes the electronic environment of the atomic site (core levels) and the occupied densities of state (valence band) below the Fermi level while XAFS probes the unoccupied densities of states in the conduction band and the extended local structure (several shells) of Si in the nanowire.

By studying bulk Si(100), silicon nanowires, and porous silicon with PES and XAFS, we can address several structure-electronic properties issues such as the densities of states below and above the Fermi level and the band gap. PES, in the single-particle picture, reveals the chemical state of the element in its core-level spectra and the electron densities of states (DOS) in its valence-band. XAFS measures the modulation of the absorption coefficient above an absorption edge. It is conveniently divided into the x-ray absorption near-edge structures (XANES) region, the first 40–50 eV above the edge, and the extended x-ray absorption fine-structures (EXAFS) region that extends to as much as 1000 eV above the edge. Si(100) and porous silicon are the

0163-1829/2000/61(12)/8298(8)/$15.00 PRB 61 8298 ©2000 The American Physical Society

two extreme cases in crystalline dimensionality for crystalline Si with the former having very-long-range order while the latter having crystalline pillars and nodules as small as a nanometer.[7] The Si nanowires studied here are strucutrally somewhere between bulk silicon and porous silicon. Thus the effect in dimensionality and degree of disorder on the electronic structure can be revealed from the densities of states, both below and above the Fermi level (probed by PES and XANES, respectively), and the local structure of Si atoms in the nanowires (probed by EXAFS).[9,10]

II. EXPERIMENTAL

Si nanowires were prepared by a laser ablation technique as described previously.[1,3,4] The system consists of a quartz tube placed inside a furnace and an excimer laser capable of delivering pulses (34 ns) energies of 400 mJ at 248 nm at a frequency of 10 Hz. A target and a water-cooled copper finger were placed inside the quartz tube. Si nanowires were produced by laser ablation of a target of Si and SiO_2 mixture. A carrying gas of Ar with 5% H_2 was used during the process [~300 torr and 50 sccm (standard cubic centimeter per minute)]. The resulting Si nanowires (henceforth denoted Si nw) were collected on the wall of the quartz tube downstream where the temperature was ~930 °C. The Si nanowires thus produced appear as a brown spongelike web which contains primarily long nanowire Si chains. Sometimes a small amount of chains of Si nanoparticles linked by amorphous oxide is also found.[4] A specimen of predominant Si nw with diamters mainly within 20–30 nm was chosen for this investigation. TEM, SEM, XRD, and Raman techniques had been used to reveal the morphology and structure.[1,3,4]

Figure 1(a) shows a TEM micrograph of the specimen. Figure 1(b) shows more detailed morphology of a Si nanowire in high resolution. It can be clearly seen that a nanowire Si chain is ~25–30 nm in diameter and is coated with several nm of silicon oxide. Crystal defects are also evident. If we leave out the oxide layer, the actual diameter of the unoxidized wire is in the range of 18–23 nm. This is ~3/4 of the nominal diameter. This is, however, considerably larger than the nanopillars and nodules in PS responsible for luminescence. For intense luminescence in the visible, the quantum confinement theory requires that the size of the Si nanostructure be less than 5 nm.[7] It is conceivable that there exist smaller grains of Si nanocrystallites in Si nw responsible for the observed luminescence.

PES measurements were performed in a vacuum generator (VG) surface analysis system, ESCALAB 2200-iXL. A monochromatic Al $K\alpha$ x-ray source (1486.6 eV) and a 150-nm hemispherical electron-energy analyzer were used. At 10-eV pass energy, the overall experimental resolution with a 250-μm spot size is ~0.45 eV. The nanowire specimen was a piece of a compressed brown spongelike web of ~3 mm across and ~2-mm nominal thickness. It was mounted onto a Mo substrate with a conducting silver paste. The as-prepared specimen was first examined without any chemical treatment. It was subsequently etched with a HF solution to remove the surface oxide. Both TEM and SEM showed that after the HF treatment, the morphology of the

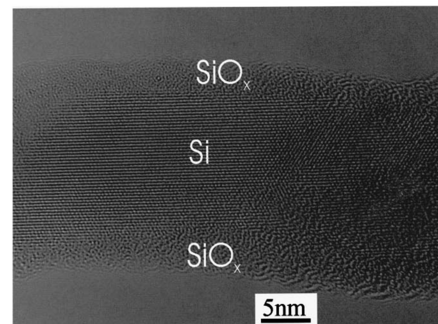

FIG. 1. (a) TEM image of Si nanowires prepared by laser ablation (upper panel). (b) A closeup image of a Si nanowire showing oxide encapsulation (lower panel).

nanowires remain essentially intact except for the removal of the surface oxide layer. This procedure sometimes leads to dissolution and fragmentation of the specimen. A *p*-type Si(100) wafer and a porous silicon (PS) sample were also examined under similar conditions. The PS specimen was prepared electrochemically using a *p*-type Si(100) wafer at a current density of 20 mA/cm^2 for 20 min. Since both PS and Si nw charged up significantly during the PES measurement, an electron flood gun was used to compensate the effect of charging. Overcompensation may sometimes occur. These situations will be discussed below.

XAFS measurements at the Si K edge (~1840 eV) were carried out at the double-crystal monochromator beamline of the Canadian Synchrotron Radiation Facility (CSRF) located at the Synchrotron Radiation Center (SRC), University of Wisconsin–Madison. InSb(111) were used as monochromator crystals. In addition to the Si nanowire, Si(100) wafer, and porous silicon, a quartz sample (crystalline SiO_2) was also studied. SRC operates at 800 MeV with a current of 250 mA at injection. Both total electron yield (TEY) and fluorescence yield (FLY) were used to obtain the absorption spectra. The incident photon flux I_0 was monitored with an in-line N_2 ionization chamber. The TEY was monitored with

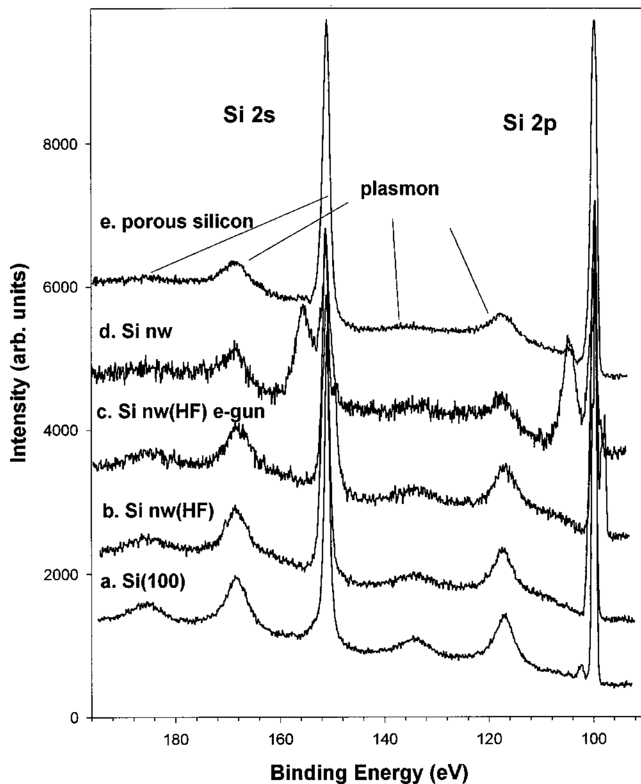

FIG. 2. Si 2*p* and 2*s* XPS spectra for the specimens: (a) HF-etched Si(100), (b) Si nw (HF, no flood gun), (c) Si nw (HF, flood gun), (d) Si oxide-encapsulated Si nw (flood gun), (e) porous silicon (flood gun). All spectra have been aligned to the Si $2p_{3/2}$ of Si(100).

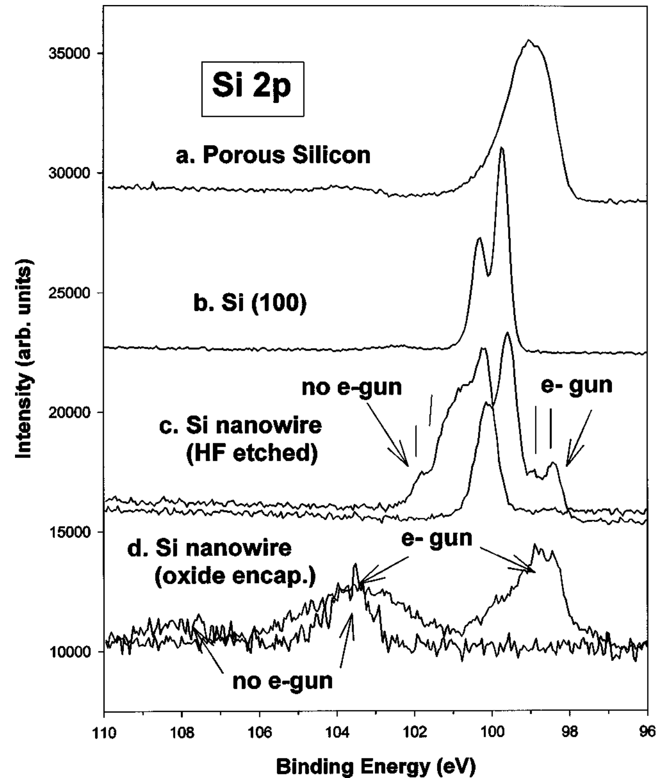

FIG. 3. Si 2*p* XPS of (a) porous silicon, (b) Si(100), () Si nw (HF), and (d) Si nw (ambient, oxide encapsulated). In (c) and (d) spectra with and without an *e*-flood gun were shown.

the specimen drained current normalized to I_0. FLY was collected with a channel-plate detector positioned at 90° with respect to the incident light. Due to the short attenuation length for inelastic scattering of the low-energy photoelectrons in the solid relative to that of the fluorescence photons, TEY enhances the signal from the surface and the near-surface region (5–10 nm) of the specimen while FLY probes the bulk (50–100 nm). Thus the combined use of TEY and FLY provides some selectivity[11] in measuring the electronic structure of different regions (depth) of the specimen.

III. RESULTS AND DISCUSSION

A. PES: Si core-level spectra

Figure 2 shows the Si $2p$ and $2s$ core-level spectra of Si(100), Si nanowires, and porous silicon recorded at 20-eV pass energy. Since charging is a problem with Si nanowires and porous silicon, all the Si $2p_{3/2}$ levels have been aligned to the Si $2p_{3/2}$ peak of Si(100) at 99.7 eV. Thus chemical shift is not always a viable option for these systems in PES measurements. Both Si(100) [Fig. 2(a)] and PS [Fig. 2(e)] were etched with HF prior to their introduction into the experimental chamber. This procedure removes the native surface oxide and passivates the surface with hydrogen. Figure 2(d) corresponds to the oxide-encapsulated Si nanowire specimen, Si nw, while Figs. 2(c) and 2(b) correspond to the HF-etched Si nw (HF) with and without the use of an *e*-flood gun.

Several features are immediately apparent from Fig. 2. First, all spectra exhibit equally spaced satellite structures at the higher binding-energy side (17.5 eV) of the main core peaks. These features are the bulk plasmons[12,13] characteristic of Si excited by the photoelectrons through an inelastic energy-loss process. Surface plasmons which are expected at ~12 eV above the main peaks for a clean Si surface are less evident. This is because the surface are all chemically modified. It is well established that surface reaction quenches the surface-plasmon signal.[14] The presence of bulk plasmons immediately indicates that all the materials in question are essentially elemental silicon although there is some broadening in Si nw and a significant broadening in PS. Second, in the Si $2s$ and $2p$ region of the Si nw spectrum, there is an intense peak at ~4 eV above the main peak. It has been established that surface Si can be oxidized by electronegative elements through several oxidation states (1–4) and the binding energy increase associated with unit increase in oxidation state is ~1 eV.[15] Thus the peak at ~4 eV above Si is attributed to SiO_2. The broadening of both the Si and SiO_2 peaks are indicative of the presence of suboxides SiO_x $(x<2)$.[15] Third, the more interesting features are seen in the spectra of the HF-etched Si nw. The spectrum [Fig. 2(b)] exhibits a shoulder at the higher binding-energy side of the main peak, it shifts to the lower binding-energy side of the main peak when an electron flood gun was used to compensate charging. These features suggest the presence of poorly conducting Si nw fragments and will be further examined below.

Figure 3 compares the Si $2p$ spectra recorded using 10-eV pass energy. The Si(100) spectrum shows a well-resolved Si $2p_{3/2,1/2}$ doublet at 99.7 and 100.3 eV, respectively. There is a barely visible peak at ~102.5 eV. It can be attribute to the presence of a small amount of surface SiO_x

and SiF_x (+2 and +3 oxidation state). The presence of a small amount of O and F was confirmed in a wide energy scan of the O and F 1s region. The porous silicon specimen shows a broad Si peak at ~99 eV and a small amount of surface SiO_2 at ~103.7 eV. The problem with nanoscale Si appears to be that due to their small size and the presence of a large surface area which is susceptible to oxidation, a fraction of the wires are in poor contact with each other and with the substrate, and therefore become nonconducting. Since the wires and/or nanostructures in the PS network have a distribution in size and some are not in good electrical contact with the network, differential charging will result in a shift to higher binding energy and a significant broadening in its core level. When an e-gun is applied, however, overcompensation will result in a shift to lower binding energy. Thus the shift of Si 2p in PS to an unusually low binding energy relative to that of Si(100) and the associated distortion can be attributed to charge overcompensation. The charging problem in the oxide-encapsulated Si wire is also severe. We see from Fig. 3(d) that the oxide-encapsulated Si nw exhibits a broad SiO_2 peak at ~4 eV above the Si peak. Without charge compensation, the entire spectrum charges up by ~5 eV. However, when HF removes the surface oxide of the Si nw, the oxide peak disappears and charging is dramatically reduced.

We now return to another interesting feature in the spectra of the HF-etched Si nw [Fig. 3(c)]. There are two sets of doublets and one appears as a shoulder to the main at higher binding energy (marked with vertical bars) when the flood gun was not used. However, when the flood gun was used (at ~0 V), the shoulder shifts to the lower binding-energy side of the main. In addition, when the voltage on the flood gun was increased to −0.5 and −1 V, the less intense doublet shifts to lower binding energy accordingly while the main peak moves little. This observation indicates that the shoulder corresponds to nanowire fragments and/or nanocrystallites electrically detached to the sponge framework during HF etching. The possibility of associating this with remaining Si oxide can be ruled out based on its narrow linewidth (oxides always exhibit considerably broader lines).

In Fig. 4, we aligned and normalized the Si 2p and 2s peak of the Si nw with those of Si(100) and then obtained the Si nw–Si(100) difference curve. It is perhaps surprising to see that these fragments exhibit a slightly smaller plasmon frequency (~16.5–16.8 eV). We believe that these observations are qualitative indicative despite a large uncertainty (0.5 eV) in the position of the satellites in the difference spectrum.

We want to explore qualitatively the implication of this observation if it can be confirmed. The question is whether or not it is possible for a material in a nanowire and/or nanocrystallite to exhibit a plasmon frequency that is smaller than that of the bulk. Plasmon oscillation arises from the collective motion of the nearly free electrons in metals and semiconductors.[12,13] Its frequency ω_p can be expressed as

$$\omega_p = (4\pi N e^2/\epsilon m^*)^{1/2}, \quad (1)$$

where N is the density of electron charge per unit volume, e is the electron charge, ϵ is the dielectric constant, and m^* is the effective mass. Two-dimensional (surface) plasmon can also exist. Its frequency ω_s is related to the bulk plasmon by

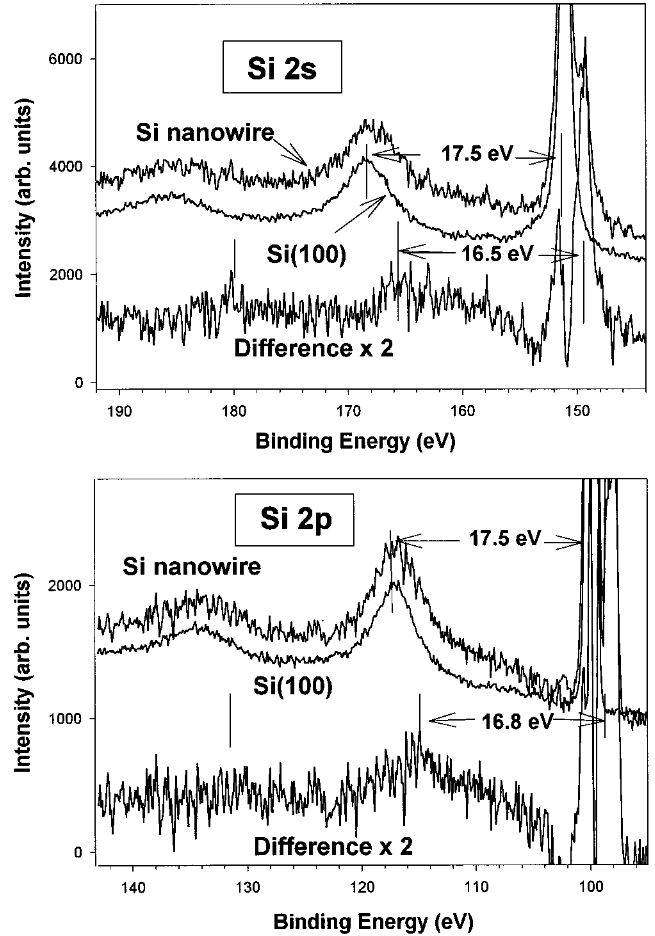

FIG. 4. Compariosn of the Si 2s and 2p regions of the HF-etched Si(100) and Si nw. The difference curve shows the spectrum of the poor conducting fragments.

$\omega_s = \omega_p/(2)^{1/2}$. It should be cautioned that these equations apply to bulk systems and provide a starting point for discussion; the difference between surface- and bulk-plasmon frequencies is influenced by dimensionality effects. For example, Sassaki *et al.*[16] reported that the plasmon frequency in porous silicon behaves more like $\omega_p/(3)^{1/2}$ than $\omega_p/(2)^{1/2}$. In the samples reported here, surface plasmon is quenched by surface oxide and/or surface hydride. Although the plasmon frequency generally take on a dispersion relationship with q (lattice vector) in low-dimension systems, the Si nanowires under investigation are mostly still of ''bulk'' character. From Eq. (1) we see that a decrease in the plasmon frequency corresponds to a drop in $(4\pi N e^2/\epsilon m^*)^{1/2}$. The terms that will likely change are the effective mass and the dielectric constant.[17,18] It has been shown that the dielectric constant of Si nanowire is larger than that of the bulk while the effective mass gets smaller than that of the bulk.[7,17,18] N may also become smaller as the fraction of electronegative oxygen atoms at the interface increase with decreasing diameter. It is plausible that a smaller plasmon frequency may exist in very small Si nanowire fragments, although more work is needed to substantiate this notion.

B. Valence-band spectra

Figure 5 shows the valence-band spectra for the HF-etched Si nanowires, Si(100), and porous silicon. The

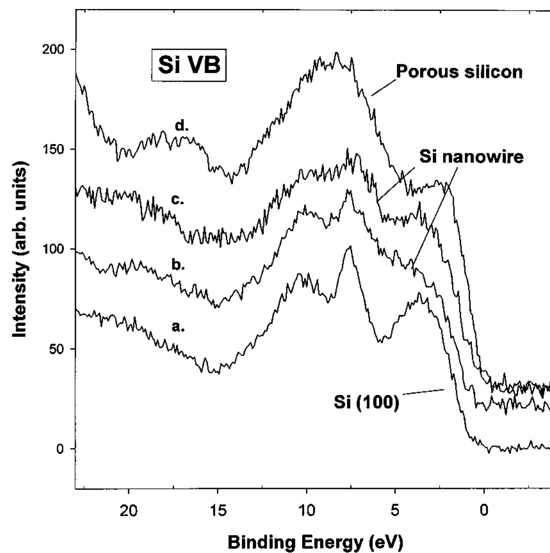

FIG. 5. Valence-band spectra of HF-etched specimens: (a) Si(100), (b), and (c) Si nw, and (d) porous silicon. Spectrum (c) was recorded with the same specimen that gave Fig. 3(c). The slightly sharper spectrum (b) was obtained from another specimen where no poorly conducting fragment was observed.

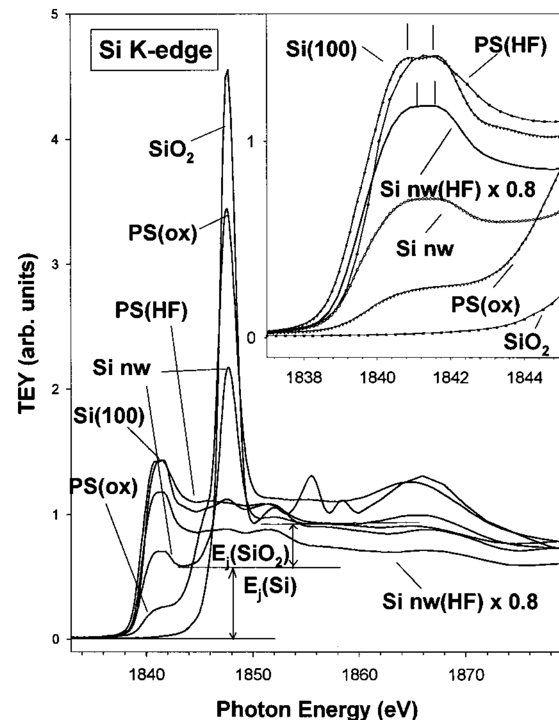

FIG. 6. TEY Si K-edge XANES for Si nw and Si nw (HF) (ambient and HF etched), Si(100), porous silicon (ambient and HF etched), an SiO_2 (quartz) normalized to unity edge jump. The edge region was expanded in the inset. The vertical arrows mark the etch jump for the Si and SiO_2 component of Si nw (ambient).

Si(100) spectrum shows a three-peak pattern characteristic of the densities of states of the *s-p* bands of silicon. Two nanowire samples were used in the measurement. The upper curve [Fig. 5(c)] was obtained from the same Si nw sample used to record Figs. 2 and 3 which indicate the presence of a small fraction of nanowire fragments in poor contact with the substrate. These wire fragments cause some broadening and a shift of the top of the valence band toward the Fermi level, as was the case in the Si $2p$ spectrum [Fig. 3(c)]. The maximum of the valence band remains more or less unchanged, however. The lower curve [Fig. 5(b)] was obtained from another HF-etched Si nw sample that did not show detached nonconducting Si nw in its core-level spectrum. It also charges up but e^--gun compensation causes no distortion. Thus the spectrum represents that of a Si nw without a surface oxide layer. The valence-band spectra observed in the Si nw spectra are similar to that of Si(100) except for a noticeable broadening. This broadening is attributed to chemical inhomogeneity due to a distribution of wires of different sizes, and disorder resulting from surface- and/or interface-induced stress and lattice distortion. The porous silicon vance band (VB) broadens further, due to the distribution of smaller interconnecting nanowires in a large network each of which exhibits a slightly different chemical environment and charging properties. It also shows some residue surface oxide signal between 15–20-eV binding energy. This observation is consistent with the broadening seen in the $2p$ core-level spectra [Fig. 3(a)]. Thus the valence-band results confirm that the Si nanowires are crystalline Si, albeit with considerable disorder.

C. Si *K*-edge x-ray absorption fine structures (XAFS)

Si K-edge XAFS arises form the excitation of a Si $1s$ electron into previously unoccupied states of p character in the conduction band. In the near-edge region the spectral features correspond to the dipole excitation of the core electron to the bound and quasibound states, and are associated with the structure and bonding environment of the absorbing atom. At higher energy above the edge, the absorption coefficient often exhibits oscillations resulting from the interference of the outgoing and the backscattered photoelectron. Since XAFS measures the photon energy of a transition, not the kinetic energy of electrons, charging is not a problem. Thus chemical shift can be measured either in terms of the edge jump threshold energy or the energy position of the first resonance (excitation to the localized unoccupied densities of states just above the Fermi level, sometimes known as whiteline).

1. Si K-edge XANES

Figure 6 shows the Si K-edge XANES for Si nw, Si nw (HF etched), Si(100), PS (HF etched), PS (oxidized in the ambient), and SiO_2 (quartz) recorded in TEY. All spectra are normalized to an edge jump of unity except that of the Si nw (HF) which was downscaled (80%) for clarity. The edge jump region was expanded in the inset. Since TEY is sensitive to the surface and the near-surface region of the specimen, surface oxide has a noticeable contribution to the total signal. Several features from Fig. 6 concerning the ambient Si nw and porous silicon are discussed below in some detail.

First, the Si(100) spectrum exhibits an intense absorption peak at the edge (whiteline) followed by a small surface oxide peak at 1847.5 eV, which corresponds to the resonance at the edge-jump onset of SiO_2. It should be noted that the native oxide on Si surface is amorphous SiO_2. It exhibits the same XANES as quartz except that the fine structures be-

tween 1847.5 and 1866 eV seen in quartz are smoothed out. The intensity of this oxide peak can be used to monitor semiquantitatively the thickness of the surface oxide. For Si(100), the oxide peak disappears after HF etching. Close examination reveals that the Si(100) whiteline is a doublet (Fig. 6 inset). This doublet is a band-structure feature and is associated with long-range order in the Si crystal.[9,10,19]

Second, the Si nw XANES exhibits both Si and SiO_2 edge with resonances similar to those of ambient Si(100), except that the SiO_2 peak intensity increases significantly due to a larger surface area and a large surface Si (oxide) atom to bulk (wire) Si atom ratio [Fig. 1(b)]. The increase in intensity of the oxide resonance becomes more dramatic in porous silicon aged in the ambient atmosphere, PS (ox), where surface oxide thickness increases further. Some suboxide signals between the Si and the SiO_2 edge are also evident. HF testament removes the surface oxide (disappearance of the peak at 1847 eV). Returning to the Si nw TEY spectrum, a measure of the relative edge jump at 1844 and 1860 eV for Si and SiO_2, respectively, shows that the as-measured SiO_2/Si ratio is ~2/5, large in comparison with the 1/4–1/3 ratio expected from Fig. 1. The apparent discrepancy is expected since TEY is more sensitive to the surface oxide than the encapsulated Si. The ratio becomes ~4/1 in the TEY of the oxidized PS. The oxide peak vanishes when the oxide was removed with HF as seen in the PS (HF) and Si nw (HF) spectrum.

Third, the most interesting comparison is seen in the edge jump region where the well-defined doublet observed in the Si(100) whiteline flattens out in both ambient and HF-etched Si nw and totally blurs into a signal peak in porous silicon (Fig. 6, inset). This observation indicates that there is already a noticeable degradation in long-range order in Si nw due to its nanodiameter and surface effect associated lattice distortion and defects. It becomes more severe in porous silicon where the doublet blurs entirely. As reported previously,[7,9,10] the PS XANES shows a blueshift in both the edge jump (point of inflection of the edge) and the position of the whiteline relative to Si(100). The blueshift has been attributed to the widening of the band gap in nm porous silicon crystallites due to quantum confinement. No noticeable edge shift is observed in the Si nw (before and after HF treatment), although the centroid of the whiteline in the Si nw XANES exhibits a small blueshift (~0.2 eV) and a broadening. We propose that this observation can be accounted for if a fraction of the Si crystallites in the nanowire in our sample exhibits the effect of quantum confinement.[20]

The above-discussed notions can be substantiated with the FLY results. It should be noted that for the Si nw of 20–30-nm diameter, FLY at the Si *K* edge is equally sensitive to the surface and the bulk of the Si nw (the one-absorption length for Si at the Si *K* edge is ~1.3 μm). In the case of a several-mm-thick Si(100) wafer, however, the FLY XANES, though sensitive almost entirely to the bulk, suffers from severe self-absorption (sometime known as the thickness effect: the fluorescence photon was reabsorbed by the specimen) since the one-absorption length of the fluorescence photon is $\sim 10^3$ nm. The thickness effect (mainly due to self-absorption) results in a reduction in whiteline intensity and significant broadening of all the features. The effect is less severe in the more porous Si nw and PS specimens.

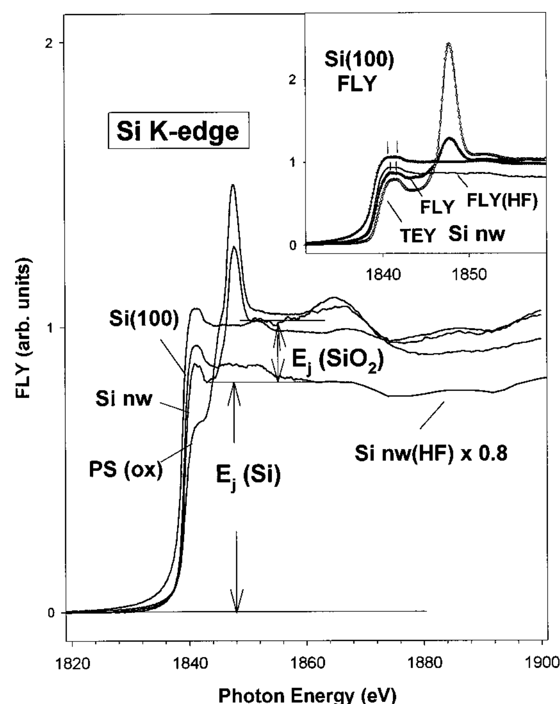

FIG. 7. FLY Si *K*-edge XANES for Si(100), Si nw, Si nw (HF), and porous silicon. The vertical arrows mark the edge jump of the Si and SiO_2 components in Si nw. Inset: Comparison of the FLY of Si(100) and Si nw (HF) and the TEY and FLY of Si nw. The Si nw (HF) spectrum was downscaled for clarity.

Figure 7 shows the FLY XANES for Si nw, Si nw (HF), Si(100), and PS (oxidized). A comparison of the TEY with the FLY XANES for the Si nw and Si nw (HF) is shown in the inset. Several points can be made here: First, the Si nw whiteline doublet is somewhat visible in the FLY indicating that the Si wire still maintains some long-range order, but the separation is significantly smaller than Si(100) and is in the direction of coalescing. Second, there clearly exhibits a blueshift of the edge jump as well as the whiteline from Si(100) to Si nw to PS. Third, the edge jump ratio SiO_2/Si in the FLY spectrum is now ~1/4 in excellent accord with the expected ratio shown in Fig. 1. Thus both TEY and FLY XANES exhibit a trend of increasing degradation in long-range order going from bulk Si to Si nw to PS.

2. Si K-edge EXAFS

The EXAFS results further confirm the above observations. Figure 8 shows the EXAFS $\chi(k)k$ (weighted by k) for Si(100), Si nw and Si nw (HF) recorded in TEY in the upper panel and the corresponding Fourier transform (FT) in the lower panel. The corresponding FLY shows similar results except for a small reduction in amplitude and poor statistics due to the thickness effect and low counting rate, respectively, and was not used for the analysis.

EXAFS (Refs. 21 and 22) arises from the interference of the outgoing and the backscattered photoelectron at the absorbing atom. This interference modulates the absorption coefficient and is dominated by single scattering at medium and high k. For an absorbing atom surrounded by N_j backscattering atoms of the same kind with a separation of r_j, EXAFS can be expressed in terms of an amplitude function A and a

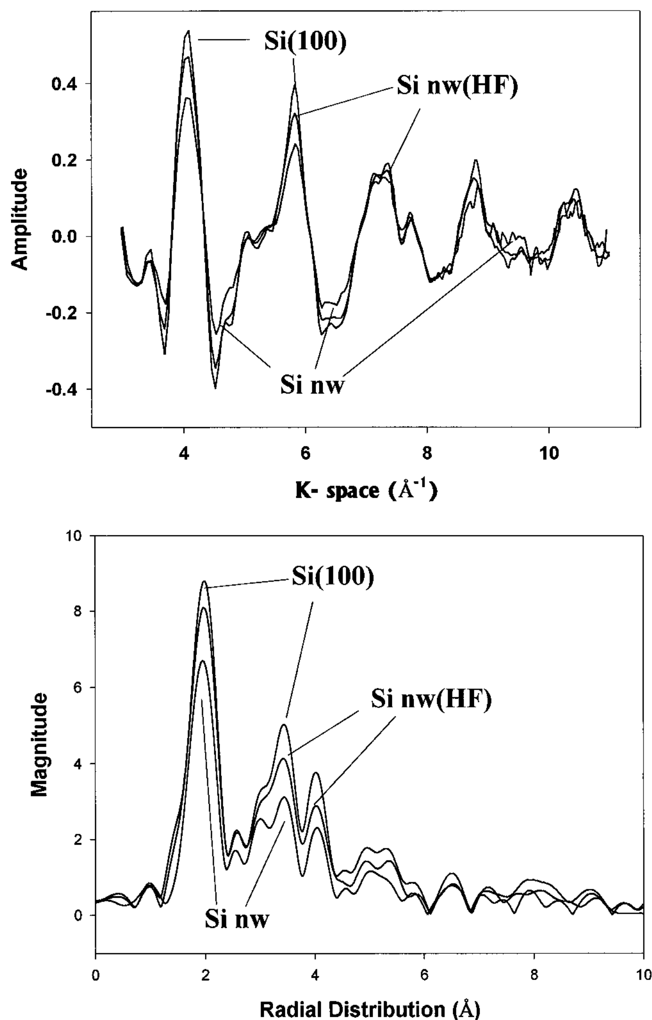

FIG. 8. Upper panel: k-weighted Si K-edge EXAFS for Si nw, Si nw (HF), and Si(100). Lower panel: Fourier transform (FT). Lines indicate the nearest shells around Si for the corresponding compounds. The Si nw (HF) was downscaled for clarity.

phase-shift function $\Phi(k,r_j,N_{j,ab})$. The amplitude A is a function of the coordination number N_j of identical neighboring atoms j with the same interatomic distance r_j, the backscattering amplitude $f(k,\pi)$ of the neighboring atom, and the mean-square displacement of the pair σ_j^2 in the form of a Debye-Waller (DW) factor, $\exp(-2\sigma j_j^2 k^2)$. The phase term $\Phi(k)=\sin(2kr_j+\phi_{j,ab})$ includes the total phase contribution $\phi_{j,ab}$, from the absorbing atom and the backscattering atom. Thus the EXAFS amplitude decreases as N_j decreases and σ_j^2 increases. σ_j^2 and hence DW measures the degree of the disorder in the lattice. σ_j^2 can be considered as a mean-square relative displacement of the interatomic distance. It may be conveniently divided in two terms:[23] $\sigma_j^2=\sigma_{\mathrm{dyn}}^2+\sigma_{\mathrm{stat}}^2\sigma_{\mathrm{dyn}}^2$ is a dynamic term. It is concerned with the thermal motion of the atoms in the lattice and is temperature dependent. σ_{stat}^2 is sometimes referred to as a static disorder term. It deals with a slightly different interatomic distance between identical pairs resulting from the presence of surface and interface atoms, surface reconstruction, grain boundary, and defects. N_j and DW are of considerable significance here because as the nanowire becomes smaller, the surface to bulk atom ratio increases and on average the coordination number of like atoms decreases. In addition, oxide encapsulation and hydrogen passivation of the Si surface (HF treatment), as well as the presence of defects, will induce lattice distortion, resulting in increasing disorder (large σ_j^2). For example, it is well known that porous silicon films are highly stressed and have large DW values.[7,9]

In the upper panel of Fig. 8, we see that the k-weighted EXAFS for Si(100), Si nw (HF) and Si nw show similar oscillations although both Si nw (before and after HF etching) exhibit a noticeable reduction in amplitude in the low-k region. This indicates a degradation in long-range order. The similarity in frequency is perhaps surprising at first glance for the ambient Si nw sample since its EXAFS should consist of two contributions: the Si nanowire and the surface oxides. It turns out Si-O EXAFS has most of its intensity at the low-k region while Si-Si EXAFS still has significant amplitude in the mid-k and high-k regions.[19] This is because the backscattering amplitude of oxygen is smaller than that of Si. Thus Si-O EXAFS damps rapidly in k space and vanishes at high k. In addition, the surface oxide is amorphous, thus it only has important EXAFS from its first shell. The EXAFS of Si nw (HF) is unquestionably that of crystalline silicon. This finding is confirmed by TEM and electron-energy-loss spectroscopy (EELS) results.[24]

The amplitude and phase have been separated by a Fourier-transform (FT) technique.[21] The FT analysis yields the radial distribution (phase adjusted of the different shells as shown in the lower panel of Fig. 8. The lines mark the Si-Si distribution maximum for the first three shells. We use the EXAFS region of $k=3.0$–10.9 Å^{-1} in the analysis in which the first peak (nearest neighbors) was filtered and backtransformed with exactly the same parameters (1.4–2.61 Å). The first-shell bond-length difference Δr, between Si nw (HF) and Si(100), was obtained by fitting the phase functions with E_0 (threshold energy where $k=0$) being an adjustable parameter. It should be noted that for chemically similar species, this is perhaps the most accurate method to get the bond-length difference.[23] The Δr thus obtained is -0.008 ± 0.005 Å with an E_0 adjustment of -0.98 eV. This observation may indicate a marginal compression of the Si lattice on average in the HF-etched nanowire under investigation. It should be noted that the relatively small uncertainty is associated with the ''bond-length difference,'' not the bond length itself. The assumption of chemical transferability of phase and amplitude is at work here (Si in bulk silicon vs Si in porous silicon). Similar analysis of the Si nw (oxide encapsulated) EXAFS shows a Δr of -0.025 ± 0.010 Å and a ΔE_0 of -2.73 eV. This observation suggests that the presence of the surface oxide leads to a small lattice contraction. We caution that this may be also due to the presence of a weak underlying Si-O EXAFS neglected in the analysis.

The upper panel of Fig. 8 shows that the reduction in EXAFS amplitude is largely in the low- and mid-k region. This is the region the Si backscattering amplitude is the largest[21] (peaks at $\sim$4 Å^{-1}). This observation suggests either a reduction in the effective coordination number on average or an increase in disorder in the Si nw. The reduction in the EXAFS amplitude is clearly seen in the FT. From the radial distribution, we can identify the interatomic distance in Si(100) and Si nw (ambient and HF etched) up to the fourth

shell. The amplitude reduction is more significant at the outer shells. A comparison of the first-shell amplitude function obtained from back FT shows a reduction in amplitude of the Si nw (HF) relative to that of Si(100). Since both materials are crystalline with identical structure locally, the reduction in amplitude is almost certainly attributable to the reduction in the effective coordination number and large root-mean-square relative displacement[26] of the interatomic distance (σ^2) in both the oxide-encapsulated and HF-etched wires. The latter is probably more important. A comparative analysis of the amplitude of the first shell of Si nw (HF) relative to Si(100) shows a ratio of the effective coordination number of 0.97 ± 0.02 and a $\Delta\sigma^2$ of 5.9×10^{-4} Å ($\sigma = 0.024$ Å). This difference is similar to some of the results obtained previously on chemically similar samples.[25] The latter is attributed to static disorder. Similar behavior in EXAFS has been observed before in porous silicon and has been attributed to the degradation of long-range order and lattice distortion.[7,9,27]

IV. SUMMARY AND CONCLUSION

We have reported a PES and XAFS study of Si nanowire specimens prepared by a laser ablation technique. The Si nanowire surface layer is found to be primarily SiO_2 and the Si wire is essentially crystalline Si with broaden densities of states both below and above the Fermi level; this behavior is attributed to the degradation of long-range order and chemical inhomogeneity resulting from its nanosize and oxide encapsulation. There is an indication that at least a fraction of the Si nw exhibit a wider band gap than that of bulk Si and that there is some local disorder and degradation of long-range order in Si nw. The PES and XAFS results using both TEY and FLY confirm previous TEM, XRD, and Raman observations.

ACKNOWLEDGMENTS

This work was partially supported by the Research Grant Council of Hong Kong and the Natural Science and Engineering Research Council (NSERC) of Canada. T.K.S. acknowledges the great hospitality of the Center of Super Diamond and Advanced Films (COSDAF) and the City University of Hong Kong. The Synchrotron Radiation Center is supported by the U.S. National Science Foundation (NSF) under Grant No. DMR-95-31009.

[1] Y. F. Zhang, Y. H. Tang, N. Wang, D. P. Yu, C. S. Lee, I. Bello, and S. T. Lee, Appl. Phys. Lett. **72**, 1835 (1998).
[2] A. Morales and C. M. Lieber, Science **279**, 208 (1998).
[3] N. Wang, Y. H. Tang, Y. F. Zhang, D. P. Yu, C. S. Lee, I. Bello, and S. T. Lee, Chem. Phys. Lett. **283**, 368 (1998).
[4] N. Wang, Y. H. Tang, Y. F. Zhang, C. S. Lee, and S. T. Lee, Phys. Rev. B **58**, R16 024 (1998).
[5] Y. F. Zhang, Y. H. Tang, Y. F. Zhang, C. S. Lee, I. Bello, and S. T. Lee, J. Cryst. Growth **197**, 136 (1999).
[6] L. T. Canham, Appl. Phys. Lett. **57**, 1046 (1990).
[7] A. G. Cullis, L. T. Canham, and P. D. J. Calcott, J. Appl. Phys. **82**, 909 (1997).
[8] B. Li, D. Yu, and S.-L. Zhang, Phys. Rev. B **59**, 1645 (1999).
[9] T. K. Sham, X. H. Feng, D. T. Jiang, B. X. Jiang, J. Z. Xiong, and A. Bzowski, Can. J. Phys. **70**, 813 (1992).
[10] S. Schuppler, S. L. Friedman, M. A. Marcus, D. L. Adler, Y. H. Xie, F. M. Ross, T. D. Harris, W. L. Brown, Y. J. Chabal, L. E. Brus, and P. H. Citrtin, Phys. Rev. Lett. **72**, 2648 (1994).
[11] S. J. Naftel, I. Coulthard, T. K. Sham, S. R. Das, and D. X. Xu, Phys. Rev. B **57**, 9179 (1998).
[12] D. Pine, *Elementary Excitation in Solids* (Addison-Wesley, New York, 1963).
[13] R. J. Elliot and A. F. Gibson, *An Introduction to Solid State Physics and Its Applications* (Macmillan, New York, 1974).
[14] R. E. Watson and M. L. Perlman, Struct. Bonding (Berlin) **24**, 83 (1975).
[15] F. J. Himpsel, B. S. Meyerson, F. R. McFeely, J F Morar, A. Taleb-Ibrahahimi, and J. A. Yarmoff, in *Proceedings of the Inrico Fermi School on '' ''Photoemission and Absorption Spectroscopy of Solids and Interfaces with Synchrotron Radiation*, edited by M. Campagn and R. Rosei (North-Holland, Amsterdam, 1990), p. 203.
[16] R. M. Sassaki, F. Galembeck, and O. Teschke, Appl. Phys. Lett. **69**, 206 (1996).
[17] M. Kumagai and T. Takagahara, Phys. Rev. B **40**, 12 359 (1989).
[18] R. J. Needs, S. Bhattacharjee, K. J. Nash, A. Qteish, A. J. Read, and L. T. Canham, Phys. Rev. B **50**, 14 223 (1994).
[19] J. C. Woicik and P. Pianetta, in *Synchrotron Radiation Research*, edited by R. Z. Bachrach, Advances in Surface and Interface Vol. 2 (Plenum, New York, 1992), p. 221.
[20] T. K. Sham, D. T. Jiang, I. Coulthard, J. W. Lorimer, X. H. Feng, K. H. Tan, S. P. Frigo, R. A. Rosenberg, D. C. Houghton, and B. Bryskiewicz, Nature (London) **363**, 331 (1993).
[21] J. J. Rehr and R. C. Alberts, Phys. Rev. B **41**, 8139 (1990).
[22] E. A. Stern, D. E. Sayer, and F. W. Lytle, Phys. Rev. B **11**, 4836 (1975).
[23] T. K. Sham, J. B. Hastings, and M. L. Perlman, J. Am. Chem. Soc. **120**, 5904 (1980).
[24] T. K. Sham, X. H. Sun, H. Y. Peng, N. B. Wong, and S. T. Lee (unpublished).
[25] T. K. Sham, Acc. Chem. Res. **19**, 99 (1986).
[26] G. Beni and P. M. Platzman, Phys. Rev. B **14**, 1514 (1976).
[27] I. Coulthard and T. K. Sham, Solid State Commun. **110**, 203 (1999).